

**Hydrocarbon Metabolism and Petroleum Seepage as Ecological and Evolutionary Drivers for *Cycloclasticus***

**Running title: *Cycloclasticus*: Hydrocarbons and Ecology**

**Authors:** Eleanor C. Arrington<sup>1</sup>, Jonathan Tarn<sup>2</sup>, Veronika Kivenson<sup>3</sup>, Brook L. Nunn<sup>4</sup>, Rachel M. Liu<sup>5</sup>, Blair G. Paul<sup>6</sup>, and David L. Valentine<sup>1,7</sup>

<sup>1</sup>Marine Science Institute, University of California, Santa Barbara, Santa Barbara, CA, USA

<sup>2</sup>Interdepartmental Graduate Program in Marine Science, University of California, Santa Barbara, Santa Barbara, CA, USA

<sup>3</sup>Innovative Genomics Institute, University of California, Berkeley, Berkeley, CA, USA

<sup>4</sup>Department of Genome Sciences, University of Washington, Seattle, WA, USA

<sup>5</sup>School of Oceanography, University of Washington, Seattle, WA, USA

<sup>6</sup>Bay Paul Center, Marine Biological Laboratory, Woods Hole, MA, USA

<sup>7</sup>Department of Earth Science, University of California – Santa Barbara, Santa Barbara, CA, USA

**Corresponding authors:** valentine@ucsb.edu and earrington@ucsb.edu

**Contact information for DLV:** Department of Earth Science and Marine Science Institute, University of California, Santa Barbara, 1006 Webb Hall, Santa Barbara, CA, 93106-9630, USA

**Contact information for ECA:** Marine Science Institute, University of California, Santa Barbara, 1006 Webb Hall, Santa Barbara, CA, 93106-9630, USA

## **Abstract**

Aqueous-soluble hydrocarbons dissolve into the ocean's interior and structure deep-sea microbial populations influenced by natural oil seeps and spills. *n*-Pentane is a seawater-soluble, volatile compound abundant in petroleum products and reservoirs and will partially partition to the deep-water column following release from the seafloor. In this study, we explore the ecology and niche partitioning of two free-living *Cycloclasticus* strains recovered from seawater incubations with *n*-pentane and distinguish them as an open ocean variant and a seep-proximal variant, each with distinct capabilities for hydrocarbon catabolism. Comparative metagenomic analysis indicates the variant more frequently observed further from natural seeps encodes more general pathways for hydrocarbon consumption, including short-chain alkanes, aromatics, and long-chain alkanes, and also possesses redox versatility in the form of respiratory nitrate reduction and thiosulfate oxidation; in contrast, the seep variant specializes in short-chain alkanes and relies strictly on oxygen as the terminal electron acceptor. Both variants observed in our work were

dominant ecotypes of *Cycloclasticus* observed during the Deepwater Horizon disaster, a conclusion supported by 16S rRNA gene analysis and read-recruitment of sequences collected from the submerged oil plume during active flow. A comparative genomic analysis of *Cycloclasticus* across various ecosystems suggests distinct strategies for hydrocarbon transformations among each clade. Our findings suggest *Cycloclasticus* is a versatile and opportunistic consumer of hydrocarbons and may have a greater role in the cycling of sulfur and nitrogen, thus contributing broad ecological impact to various ecosystems globally.

**Keywords:** Petroleum, hydrocarbons, metagenomics, oil spills, alkanes, comparative genomics, microbial ecology

## Introduction

Much of the petroleum entering the ocean annually is introduced near the seafloor from human-caused incidents such as pipeline ruptures, well blowouts, and leaking submerged oil tankers, alongside other deep hydrocarbon inputs originating from natural oil seepage and hydrothermal vents. Following petroleum release to the seafloor, several compounds dissolve into seawater due to their aqueous solubility, subsequently affecting the microbial community within the surrounding water column [1–3]. These semi-aqueous soluble compounds can be overlooked as drivers of microbial metabolism in the deep community because these compounds often evaporate from surface oil slicks exposed to the atmosphere, which receive the majority of attention from agencies and scientists responding to oil-related incidents. This work focuses on the semi-aqueous-soluble compound *n*-pentane, which is known to partition to the deep ocean following release from the seafloor [2, 3].

Petroleum exposure to seawater substantially decreases prokaryotic diversity due to a strong selection for hydrocarbon-degrading microorganisms and toxic effects on other taxa [4, 5]. Models of in-situ hydrocarbon biodegradation indicate that as a water parcel encounters a hydrocarbon source, a seed population of hydrocarbon degraders grows

abundantly [6–11]. The origin and ecology of these seed populations are primarily hypothetical. Many studies have suggested seed populations are prolonged and sustained by hydrocarbon substrates originating from various sources, including hydrothermal vents [12], cyanobacteria, and eukaryotic phytoplankton [12–14], as well as natural gas seepage [15, 16]. As an example, the ubiquitous alkane degrader, *Alcanivorax*, exhibits basal cell populations that range from 10 to 5,000 cells per mL in uncontaminated seawater [6, 17], with recent work suggesting high native abundance is subsidized by widespread biosynthesis of long-chain *n*-alkanes by marine phytoplankton [13, 18]. Other recent evidence has shown that methanotrophs can be physically transported on bubbles from a gas seep [19, 20], pointing to seeps as a physical mechanism to seed the water column with hydrocarbon degraders. Alternatively, facultative hydrocarbon degraders could be present that rely on other metabolic inputs such as amino acids, carbohydrates, lipids, or other organic acids and switch to hydrocarbons under appropriate conditions [21–23]. Very few studies have focused on how these factors control the development of a petroleum-degrading community during oil spills in previously uncontaminated waters.

Our investigation [18] of the ocean's biological hydrocarbon cycle revealed the microbial response to *n*-pentane is structured by proximity to seepage (Fig. 1). This previous work and our current study focus on sea-going incubations conducted with water collected from the deep ocean (1,000 m) along a transect spanning the Gulf of Mexico (GOM) and the North Atlantic. *n*-Pentane metabolism was observed through a closed-system optical oxygen technique. Blooms were designated as present when three consecutive time points exhibited oxygen loss greater than  $0.21 \mu\text{M h}^{-1}$  after normalization to unamended controls. This definition was based on the finding that each incubation that met this threshold continued to see oxygen decline at this rate or greater until reaching near hypoxic conditions, suggesting a bloom-like state. We observed distinct bloom response times to *n*-pentane in relation to natural seepage, whereby bloom onset on

pentane is ~9X faster in the seep-ridden Northwest Gulf of Mexico compared to the water underlying the North Atlantic subtropical gyre [18, 24]. Median bloom times varied from 72.9 days furthest from natural seepage to 8.3 days closest to natural seepage. The fraction of samples that exhibited a bloom response also coincided with proximity to natural seepage, with 100% of incubations blooming within 30 days near seepage, 33% blooming further from seepage in the northeastern Gulf of Mexico, and 0% of incubations blooming outside the Gulf within that same timeframe (Fig. 1b). While this previous work focused on the timing and occurrence of respiratory blooms on *n*-pentane, the study did not explore which microorganisms were responsible for *n*-pentane consumption or how natural seepage influences which microorganism responds in each of these settings.

Here, we investigate the influence of biogeography on microbial hydrocarbon metabolism by analyzing the genomic content of organisms with contrasting bloom responses and source water origins within the Gulf of Mexico (GOM). We extract and analyze blooms' 16S rRNA gene content, assemble high-quality draft metagenome assembled genomes (MAGs) from bloom experiments, and perform a complementary proteomic analysis to evaluate metabolism. The predominant microbial member of the *n*-pentane-enriched community across the Gulf of Mexico belongs to the *Cycloclasticus* genus, initially named for their metabolic capability to consume polycyclic aromatic hydrocarbons (PAHs). *Cycloclasticus* belongs to the class *Gammaproteobacteria* and is often detected to be abundant in oil-rich oceanic regions [25–27]. *Cycloclasticus* has also been found as a symbiont in the tissues of mussels and sponges at deep-sea oil seeps, where they likely metabolize short-chain alkanes [15, 26–29]. All cultures of *Cycloclasticus* have been isolated on aromatic substrates and are closely related according to 16S rRNA gene phylogeny [15, 25, 30–32]. We observe two strains of *Cycloclasticus* bloom in response to short-chain alkanes in the Gulf of Mexico, with one strain favoring the seep-influenced region of the northwestern GOM (hereafter referred to as the seep variant, SV).

In contrast, the other strain favors the open ocean region far from natural seepage (hereafter referred to as the open ocean variant, OOV).

## Materials and Methods

### Incubation design and sample collection

Seawater samples were collected on two research cruises aboard RV Atlantis in June 2015 and the RV Neil Armstrong in May 2017. *n*-Pentane incubations were conducted at stations 1 (40° 9.14' N, 68° 19.889' W), 2 (33° 58.21' N, 69° 43.38' W), 3 (27° 30.41' N, 87° 12.41' W), 4 (27° 15.00' N, 89° 05.05' W), 5 (27° 11.60' N, 90° 41.75' W) and 6 (27° 38.40' N, 90° 54.98' W) with seawater collected from 1,000 m. Respiration data and methods are available from [18], with sample numbers re-named for this study to exclude irrelevant data. Seawater collected from the CTD Niskin bottles was transferred to 250 mL glass serum vials using a small length of Tygon tubing. Vials were overflowed for at least 3 volumes of water and no air bubbles were present before sealing with polytetrafluoroethylene (PTFE) coated chlorobutyl rubber stopper and crimp cap seal. All bottles, except for unamended blank controls, immediately received 10  $\mu$ L of *n*-pentane using a gas-tight syringe (Hamilton) and were maintained in the dark at in-situ temperature (4 °C). Before filling, each serum bottle was fixed with a contactless optical oxygen sensor (Pyroscience) on the inner side with silicone glue, and afterward were cleaned from organic contaminants with triple rinses of ethanol, 3% hydrogen peroxide, 10% hydrochloric acid, and MilliQ water, and were sterilized via autoclave. Oxygen concentration was monitored approximately every 8 hours with a fiber optic oxygen meter (Pyroscience). Observed changes in oxygen content were normalized to unamended controls to correct for oxygen loss from background respiration processes and variability due to temperature changes. After 27-30 days, each incubation was sacrificially harvested, samples were collected for nutrient analysis and cell count analysis, and the remaining seawater was filtered on a 0.22  $\mu$ m polyethersulfone filter and stored at -80°C until further analysis.

### **Nutrient and cell enumeration**

Before filtration, seawater was collected from incubations for cell enumeration via flow cytometry and nutrient analysis. 2 mL subsamples for prokaryotic cell abundance were fixed with 0.2% paraformaldehyde and quantified using the Millipore Guava EasyCyte 5HT flow cytometer as in [33]. The dissolved nutrient (nitrate, phosphate, and ammonia) sample collection was conducted following the requirements of the University of California, Santa Barbara Marine Science Institute Analytical Lab. Seawater incubation samples were filtered through a 0.2  $\mu\text{m}$  polyvinylidene (PVDF) filter into triple-rinsed plastic HDPE 20 mL vials. Nutrient sample volumes were  $\sim$ 17 mL water and stored frozen at  $-20^{\circ}\text{C}$  until analysis. Dissolved nutrient concentrations were analyzed by flow injection analysis (FIA) using the QuikChem 8500 Series 2 (Lachat Instruments).

### **Deepwater Horizon archival sample**

We extracted and analyzed two replicate archive environmental DNA samples collected from the Deepwater Horizon event on May 30th, 2010 from a depth of 1,090 m while the wellhead was still leaking into the Gulf of Mexico. Microbial biomass was filtered onto 0.2-micron Sterivex filters (Millipore) and stored at  $-80^{\circ}\text{C}$  until further analysis.

### **DNA extraction, PCR amplification, and 16S rRNA gene analysis**

DNA was analyzed from stations within the GOM and the DWH archival samples. DNA extraction was performed from  $\frac{1}{4}$  of each filter using the PowerSoil DNA extraction kit with the following modifications: 200  $\mu\text{L}$  of bead beating solution was removed at the initial step and replaced with phenol-chloroform, the C4 bead binding solution was supplemented with 600  $\mu\text{L}$  of 100% ethanol, and we added an additional column washing step with 650  $\mu\text{L}$  of 100% ethanol. Extracts were purified and concentrated by ethanol precipitation, then stored at  $-80^{\circ}\text{C}$ . The V4 region of the 16S rRNA gene was amplified, and each sample was barcoded as previously desc [34] with the 515F-Y and 806RB primers as previously published [35–37]. Amplicon PCRs contained 1  $\mu\text{L}$  of template DNA, 2  $\mu\text{L}$  of forward primer,

2  $\mu$ L of reverse primer, and 17  $\mu$ L of AccuPrime Pfx SuperMix. Thermocycling conditions consisted of 95°C 2 min, 30 cycles of 95°C for 20 secs, 55°C for 15 secs, 72°C for 5 min, and a final elongation at 72°C for 10 min. Sample DNA concentrations were normalized using the SequelPrep Normalization Kit, cleaned using the DNA Clean and Concentrator kit, visualized on an Agilent TapeStation, and quantified using a Qubit Fluorometer. Samples were sequenced at the UC Davis Genome Center on the MiSeq platform (Illumina) with 250 nucleotide paired-end reads. A PCR-grade water sample was included in extraction, amplification, and sequencing as negative control to assess for DNA contamination.

Trimmed fastq files were quality filtered using the `fastqPairedFilter` command within the `dada2` R package, version 1.9.3 [38] with following parameters: `truncLen=c(190,190)`, `maxN=0`, `maxEE=c(2,2)`, `truncQ=2`, `rm.phix=TRUE`, `compress=TRUE`, `multithread=TRUE`. Quality filtered reads were dereplicated using `derepFastq` command. Paired dereplicated fastq files were joined using the `mergePairs` function with the default parameters. A amplicon sequence variant (ASV) table was constructed with the `makeSequenceTable` command, and potential chimeras were removed denovo using `removeBimeraDenovo`. Taxonomic assignment of the sequences was done with the `assignTaxonomy` command using the Silva taxonomic training dataset formatted for DADA2 v132 [39, 40]. If sequences were not assigned to the Silva database, they were left as NA.

### **Metagenomic sequencing and reconstruction**

Metagenomic library preparation and high-throughput sequencing were conducted at the University of California Davis DNA Technologies Core. DNA was sequenced on the HiSeq4000 (Illumina) platform, producing 150-base pair (bp) paired-end reads with a targeted insert size of 400 bp. Quality control and adaptor removal were performed with Trimmomatic [41] (v.0.36; parameters: leading 10, trailing 10, sliding window of 4, quality

score of 25, minimum length 151 bp) and Sickle [42] (v.1.33 with paired-end and Sanger parameters).

10-70% of the trimmed high-quality reads were randomly subsampled to deconvolute assembly and downstream binning in samples with very high coverage, as in [43]. Subsamples of each metagenomic dataset were tested in increments of 10% to determine which percentage produced the highest quality *Cycloclasticus* MAG based on completion, redundancy, and number of scaffolds in the genome. The exception is sample “Cycloclasticus\_sp\_3\_C5\_1”, which was tested in increments of 5% subsampled reads to reduce the number of scaffolds in the MAG to 1. The final subsampled percentage for each sample is noted in Supplementary Dataset S4. The program dRep was used to dereplicate all MAGs created from each subsampled dataset using default parameters, which group genomes based on initial 90% MASH (MinHash distance) clustering and the 95% average nucleotide identity [44]. Only one dereplicated MAG was recovered from each sample except the DWH sample.

The subsampled high-quality reads were assembled using metaSPAdes [45] (v.3.8.1; parameters  $k = 21, 33, 55, 77, 88, 127$ ). The quality of assemblies was determined using QUAST [46] (v.5.0.2 with default parameters). Sequencing coverage was determined for each assembled scaffold by mapping high-quality reads to the assembly using Bowtie2 [47][48] (v.2.3.4.1; default parameters) with Samtools [49] (v.1.7). Contigs greater than 2,500 bp were manually binned using Anvi'o with Centrifuge (v.1.0.1) based on coverage uniformity and GC content (v.5) [50, 51]. Quality metrics for metagenome-assembled genomes (MAGs) were determined using CheckM [52] (v.1.0.7; default parameters). The taxonomy of each MAG was classified using GTDB-Tk (v.1.0.2) against The Genome Taxonomy Database [53] (<https://data.ace.uq.edu.au/public/gtdb/data/releases/release89/89.0/>, v.r89). The average

nucleotide identity of each genome was determined with the ANI Matrix via the Enveomics tool collection[54].

We reconstructed high-quality metagenome assembled genomes (MAGs) from five pentane bloom samples, with completeness >97% and redundancy <2% (black stars in Fig 2). Three MAGs, named “6\_C5\_1”, “6\_C5\_2”, and “6\_C5\_3”, originated from station 6 (natural seep region), and two MAGs, named “3\_C5\_1” and “3\_C5\_2”, originated from station 3 (open ocean region). Based on the 16S rRNA gene analysis of the two DWH samples from this study, two variants of *Cycloclasticus* were present in the sample sequenced for metagenomics. For the DWH metagenome, the second variant related to OOV could not be recovered with metagenomics due to issues with assembly fragmentation and binning of the two closely related strains. To obtain a high-quality draft MAG of “MAG\_DWH\_1”, we subsampled our reads by 50% until the OOV-related sequences were a small fraction of the assembled data.

The program dRep was used to dereplicate all MAGs reconstructed in this study using default parameters, which group genomes based on initial 90% MASH (MinHash distance) clustering and the 95% average nucleotide identity [44], which created two clusters of essentially identical genomes with “6\_C5\_1”, “6\_C5\_2”, and “6\_C5\_3” in one cluster and “3\_C5\_1” and “3\_C5\_2” in the other cluster. We also tested whether automated binning with MetaBAT2 [55] would alter the resulting MAGs but found that dRep also clustered MAGs derived from the two different binning methods as essentially identical. We further note each MAG was recovered from biologically independent incubations, yet every component of metabolism and taxonomic marker analyzed was nearly identical within each ecotype variant; therefore, we will refer to “SV-MAG” as the three MAGs from station 6 and “OOV-MAG” as the two MAGs from station 3. We also downloaded single amplified genomes (SAGs) from the Joint Genome Institute that originated from the Deepwater Horizon event under the accession numbers 2599185270, 2599185276, 2599185294.

## Other metagenomic reconstructions

Using a 16S rRNA gene search tool through the Joint Genome Institute- Integrated Microbial Genomes and Microbiomes (JGI-IMG) portal, we identified public environmental metagenomic datasets with *Cycloclasticus* representation. These datasets were downloaded, and metagenomic reconstruction was performed according to the above protocol with the following modifications: binning was performed using the automated binning software MetaBAT2 [55]. Each *Cycloclasticus* MAG recovered was manually refined with Anvi'o based on coverage uniformity and GC content (v.5), [50, 56]. See the acknowledgments section regarding the origin of the Groves Creek Salt Marsh MAGs.

## Annotation

Open reading frames were predicted for MAGs using Prodigal [57] (v.2.6.3; default parameters). Functional annotation was determined using HMMER3 [58] (v.3.1b2) against the Pfam database [59] (v.31.0) and TIGRFAM database [60] (v.15) with an expected value (e-value) cutoff of  $1 \times 10^{-7}$ , as well as the KofamScan (v.1.1.0) [61] against the Hidden Markov model (HMM) profiles for Kyoto Encyclopedia of Genes and Genomes and Kegg Orthology (KEGG/KO) with the adaptive score thresholds associated with each KO.

## Phylogenetics

To define genome phylogenomic relationships of MAGs, 16 universal ribosomal proteins (RPs) were used L2-L6, L14-L16, L18, L22, L24, S3, S8, S10, S17, and S19. This dataset was not dereplicated using dRep to show variability in metabolism among closely related *Cycloclasticus* MAGs/genomes. For phylogenies of metabolic genes and ribosomal proteins, all representative sequences and concatenated alignments containing <25% informative sites were excluded in tree construction. For phylogenetic trees of the PQQ-dependent alcohol dehydrogenase protein family, 16S rRNA gene, DMSO protein superfamily, and the copper-bound membrane monooxygenase (CuMMO) protein superfamily, all sequences used are in Supplementary Dataset S6 and Supplementary

Dataset S7. Genomes under “genome accession” were downloaded from NCBI or JGI and annotated according to the above “Annotation” section. The 16S rRNA genes were detected from the *Cycloclasticus* genome/MAG collection with RNAmmer [66]. Among the collection of genomes used in this study, accession “TIGR03080” was used to find CuMMO/particulate hydrocarbon monooxygenase proteins, “TIGR01580” was used to find *narG* proteins, and the accession “PF01011” was used to find PQQ-dependent alcohol dehydrogenase proteins. In all phylogenetic trees, each protein was aligned using MUSCLE (v.3.8.425) [62]. All columns with >95% gaps were removed using TrimAL [63]. Maximum-likelihood phylogenetic analysis of concatenated alignment was inferred by RAxML [64] (v.8.9; parameters: raxmlHPC -T 4 -s input -N autoMRE -n result -f a -p 12345 -x 12345 -m PROTCATLG). The resulting trees were visualized using FigTree [65] (v.1.4.3).

### **Metaproteomics**

We analyzed metaproteomes from two of the OOV (open ocean variant) samples with corresponding MAGs (“3\_C5\_1” and “3\_C5\_2”) as the reference databases. Proteins from each sample were extracted and prepared from ¼ filter (equivalent to ~60 mL of filtered water and ~1.3x10<sup>8</sup> bacteria) for liquid chromatography and tandem mass spectrometry (LC-MS/MS) using a protocol adapted from [67]. Briefly, filters were cut into 2 mm pieces and submerged in 100 µL of 6M urea and 600 µL of 50 mM NH<sub>4</sub>HCO<sub>3</sub> and sonicated with a Branson 250 Sonifier; 20 kHz, 5 x 20 sec on ice to lyse cells. Protein concentrations for each sample were quantified in triplicate using a Bicinchoninic Acid protein assay kit (Pierce Thermo Scientific) using a microplate reader. Proteins within the lysate were reduced and alkylated using dithiothreitol and iodoacetamide, respectively, digested with Trypsin (12 h; 1:20 enzyme to protein) and desalted with C18 centrifugal spin columns. Peptides were dried down and resuspended in 2% ACN, 0.1% formic acid before analysis with a nanoAcquity UPLC (Waters Corp., Milford, MA) in line with a Q-Exactive-HF (Thermo Fisher Scientific, Waltham, MA). Reverse phase chromatography was achieved

using a PicoTip (New Objective) fused silica capillary column (75  $\mu\text{m}$  i.d., 30 cm long) packed with C18 beads (Dr. Maisch ReproSil-Pur; C18-Aq, 120  $\text{\AA}$ , 3  $\mu\text{m}$ ). The analytical column was preceded by a 150  $\mu\text{m}$  i.d. PicoFrit (New Objective) precolumn packed with C-18 beads to 3 cm long (Dr. Maisch ReproSil-Pur; C18-Aq, 120  $\text{\AA}$ , 3  $\mu\text{m}$ ). Peptides were eluted using a 90-minute acidified (formic acid, 0.1% v/v) water-acetonitrile gradient (2-45% acetonitrile).

Sample analyses on the MS were randomized to reduce batch effects, and quality control (QC) peptide mixtures were analyzed every six injections to monitor chromatography and MS sensitivity. Each sample was analyzed with data-dependent acquisition (DDA). From precursor ion scans of 400–1200  $m/z$  the top 20 most intense ions were selected for MS2 acquisition. Centroid full MS resolution data was collected at 70,000 with AGC target of  $1 \times 10^6$  and centroid MS2 data was collected at resolution of 35,000 with AGC target of  $5 \times 10^4$ . Dynamic exclusion was set to 20 seconds and +2, +3, +4 ions were selected for MS2 using DDA mode. Comet [68, 69] was used to search the DDA files against the 2 MAGs concatenated with 50 common contaminants and the QC peptides. Comet parameters included: 10 ppm precursor mass tolerance, fully-tryptic specificity with 0 allowed missed cleavages, cysteine modification of 57 Da and modifications on methionine of 15.999 Da. PeptideProphet was used to validate peptide spectral matches (PSMs) and determine thresholds for a false discovery rate [70]. All relevant peptide hits with an e-value less than 0.01 were used to define protein presence. All peptides' tandem mass spectra discussed here were manually investigated to verify b and y ions.

### **Read-recruitment analysis**

To better understand the biogeography of OOV-MAG and SV-MAG, we searched a representative genome from each variant against the Branchwater web interface to learn which datasets among millions of global metagenomes indexed by Branchwater contain matches filtered to 0.97 cANI to either genome[71]. All projects matching OOV-MAG or SV-

MAG were downloaded and trimmed (according to the above parameters). To evaluate the prevalence of *Cycloclasticus* MAGs and single amplified genomes (SAGs) across these metagenomic datasets (including the Deepwater Horizon event), we first dereplicated the genomes/MAGs with stringency of 95% average nucleotide identity using dRep [44], then used Bowtie2 for read mapping [47][48] (v.2.3.4.1; default parameters) and analyzed the mapped reads using stringent parameters from InStrain [72]; namely we filtered reads based on 92% similarity and only noted a genomes' presence when they achieved >20% breadth (meaning at least 20% of the genome was detected), and the expected breadth was within 20% of the observed breadth (indicating the reads were mapped randomly across the genome) [65].

## Results and Discussion

### Variant biogeography

Incubations conducted with seawater from 1,000 m depth containing ambient nutrients successfully exhibited robust blooms of bacteria when supplied with *n*-pentane as a carbon and energy source. Blooms are characterized by bacterioplankton abundance, increasing by ~10X compared to unamended controls (Supplementary Dataset S1), drawdowns in inorganic phosphate and nitrate concentration (Fig. 2c, Fig. 2d, Fig. 2e; Supplementary Dataset S1), and the emergence of dominant taxa comprising >70% of the microbial community at the termination of the experiment (Fig 2a). Community analysis of incubations that failed to bloom within the experimental timeframe (27-30 days) revealed instances where the community was dominated by a limited number of taxa, indicating a microbial community shift precedes major respiratory signals (Supplementary Dataset S2, Supplementary Information Fig. S3). Over 60% of all *n*-pentane blooms in the deep GOM were dominated by the *Cycloclasticus* genus (Fig 2a). Variation among replicate incubations was observed as a change in the dominant taxa, which occurred more often at stations closer to natural seepage, potentially related to greater microbial diversity and

abundance of alkane degraders in those waters. At Station 6, *Colwellia* and an unclassified genus belonging to *Cellvibrionaceae* bloomed, and the same unclassified *Cellvibrionaceae* bloomed at Station 5 (Fig 2a).

Our data show a difference in the frequency of incubations that bloom between Station 3, located further from seeps, and Station 6, situated within a dense seep field. At Station 3, only two out of six replicates bloomed within 30 days, while at Station 6, all six replicates bloomed within the same timeframe. Our interpretation of these data is *n*-pentane degraders are less concentrated in seawater collected further from seeps, leading to inconsistent bloom patterns. While Station 5 is among the seep fields in the Northwestern GOM (Fig. 1a), it also has an inconsistent bloom response, with only 50% of incubations blooming within 30 days. This may be explained by the western flow of eastern sourced seep-deplete waters observed at the time seawater was collected (Supplementary Data Fig. S7). Collectively, bloom kinetic data and the direction of deep ocean currents indicate Station 6 likely experienced a strong and recent influence from natural seepage.

Among the blooms, we identified two dominant *Cycloclasticus* variants. One, called the “seep variant” (SV), was the primary blooming population at Station 6, located within the northwestern GOM seep field. The other, termed the “open-ocean variant” (OOV), was the primary blooming organism at Station 3, the more offshore petroleum-depleted region (Fig. 1a, Fig. 2a, Supplementary Data S3). The distribution of SV and OOV was more varied at Stations 4 and 5, with both variants present at Station 4, but only OOV blooming at Station 5 (Fig. 2a). In incubations enriched with *n*-pentane and sequenced for 16S rRNA gene analysis—regardless of bloom status—OOV was found to be more than 10% abundant in five of eight incubations from Stations 3-5 (Supplementary Information, Fig. S3), indicating its numerical dominance in areas with patchy bloom patterns. In contrast, SV was detected in only two of the eight incubations. While we refer to these variants as 'SV, seep variant' and 'OOV, open-ocean variant,' it is important to note that each may occur across these

environments, though we found them to be numerically dominant in their respective settings. A read-recruitment analysis showing the distribution of both SV-MAG and OOV-MAG across the Gulf of Mexico further supports this interpretation (Supplementary Dataset S5 and Supplementary Information Fig. S9).

Cell-specific respiration is higher for SV than the OOV (Fig. 2b). The respiration profile (Fig. 1c) of these variants also showed distinct patterns, where OOV presents more gradual oxygen consumption with time. The OOV was also observed in small relative abundances (<1%) at Station 6 (Supplementary Dataset S2). In each *n*-pentane incubation where the two variants co-occurred, the SV numerically dominated by ~3 orders of magnitude except for the *Colwellial/Cellvibrionaceae* bloom at Station 6, where both variants were detected at <1% abundance. This suggests that SV is better adapted to conditions associated with natural seepage, as it outcompeted OOV, which only bloomed at stations that are distant from seeps.

### **Pentane metabolism**

Within both SV- and OOV-MAGs, we found genomic potential for *n*-pentane utilization for catabolism and anabolism (Fig. 3). Our analyses were further supported by proteomic analysis of the OOV-MAG from Station 3 (gray stars in Fig. 2a; Fig 4b). The first step in the consumption of *n*-pentane is the oxidation to pentanol, and we hypothesize that this step is catalyzed by the copper-containing membrane-associated monooxygenase, called particulate hydrocarbon monooxygenases (*phmo*). The most well-characterized *phmo* is the particulate methane monooxygenase, which oxidizes methane to methanol [73]. *phmo* has never been demonstrated to act on *n*-pentane, though it has shown activity on *n*-butane in previous work [74]. We found multiple copies of genes encoding *phmo* in both *Cycloclasticus* MAG variants (Fig. 3, Fig. 4, Supplementary Information Fig. S8).

Each copy of *phmo* varies phylogenetically from the other copies within the same MAG, suggesting each operon may have different substrate specificities or capitalize on

alkanes of varying substrate concentrations [75] (Fig. 4). Both MAG-SV and MAG-OOV have *phmo* sequences that form monophyletic clades with reference sequences with demonstrated affinity for ethane and butane. Both variants also contain a sequence that forms a monophyletic clade that is only distantly related to a *pmmo* (particulate methane monooxygenase); however, this clade contains no currently validated reference sequences, and we refer to its function as “unknown.”. Proteomics confirmed the expression of *phmo*, specifically subunits a and b (Fig. 3, Fig. 4) in the presence of pentane. The two *phmo* genes for which peptides were detected in OOV belong to a sequence from OOV-MAG in the “unknown” clade of *phmos* and one clade containing reference sequences with a demonstrated affinity for ethane and butane. The only detected hydrocarbon monooxygenase in SV-MAG is the *phmo*, supporting the hypothesis that this enzyme functions on *n*-pentane. *AlkB*, a gene known to function on medium to long-chain alkanes, was found encoded in the MAG-OOV; however, no peptides were observed in the proteomics analyses (Fig. 3). Still, given the minimal sample size analyzed for proteomics and the potential for false negatives due to e.g. ionization and extraction efficiencies, we do not exclude the possibility that *alkB* could also be active in these samples and used to consume *n*-pentane by the OOV.

The second step in the consumption of pentane is the conversion of pentanol to an aldehyde. In many bacteria that oxidize alcohols, this reaction is catalyzed by pyrroloquinoline quinone-dependent alcohol dehydrogenases (*pqq-adh*). We found genes encoding *pqq-adh* in both *Cycloclasticus* MAG variants and proteomic expression of PQQ-ADH in OOV-MAG samples. (Fig. 3, Supplementary Information Fig S2). None of the *pqq-adh* genes formed a monophyletic clade with reference sequences known to act on methanol, providing evidence against methane metabolism in SV and OOV. In the third step of *n*-pentane consumption, the aldehydes are oxidized to carboxylic acids, which could be achieved via a tungsten-containing aldehyde ferredoxin oxidoreductase (*aor*), known to

use short-chain alkane-derived aldehydes as their substrate [15, 76]. This conversion can also be performed by *pqq-adh*, as activity on aldehydes has been confirmed with reference sequences related to those encoded by SV and OOV (Supplementary Information Fig S2). Here, pentanoate is likely beta-oxidized using acyl-CoA dehydrogenase and enoyl-CoA hydratase and shunted into central carbon metabolism via the citric acid cycle (Fig. 3).

### Differences in variant metabolic potential

The metabolic capabilities of the SV-MAG and OOV-MAG differ substantially (Fig. 3, Fig. 4). The OOV-MAG encodes for general hydrocarbon metabolism that includes the nearly complete pathway for toluene consumption via the toluene monooxygenase conversion of toluene to benzoate (7 of 8 genes), benzoate conversion to catechol (3 of 4 genes), and the catechol meta-cleavage to acetyl-CoA which enters the tricarboxylic acid cycle (13 of 13 genes). The OOV-MAG also encodes toluene 2-monooxygenase, which converts benzene to catechol (6 of 6 genes) that can also be shunted through the same catechol meta-cleavage pathway as toluene to form acetyl-CoA (13 of 13 genes) and enter the tricarboxylic acid cycle. The OOV could also use the toluene-2 monooxygenase system to convert toluene to 3-methylcatechol (6 of 6 genes) and then convert 3-methylcatechol to acetyl-CoA and shunt to the tricarboxylic acid cycle (3 of 5 genes). Furthermore, the OOV-MAG encodes for *alkB* (1 of 1 gene), which is commonly used by other organisms for consumption of long-chain alkanes via beta-oxidation (OOV encodes 7 of 7 genes), resulting in propionyl-CoA and acetyl-CoA, which are also incorporated into the tricarboxylic acid cycle. Neither OOV-MAG or SV-MAG (or any other *Cycloclasticus* MAGs analyzed in this study) encode a complete canonical naphthalene degradation pathway (naphthalene 1,2, dioxygenase is missing from all genomes/MAGs), yet the strain *Cycloclasticus* SP-1 has been experimentally validated to use naphthalene as a sole carbon source (Fig. 5b) [28]. *Cycloclasticus* SP-1 and OOV-MAG encode 3 of 10 genes for naphthalene

degradation, which indicates that OOV-MAG can also likely metabolize naphthalene, whereas SV encodes 0 of 10 genes.

Overall, the SV-MAG lacks many metabolic pathways for longer-chain alkanes and aromatic compounds compared to the OOV-MAG, seemingly limiting its hydrocarbon metabolism potential (Fig. 4, Fig. 5b). These observed differences are consistent with SV specialization on short-chain, aqueous-soluble alkanes and biogeography that includes seeding from the petroleum-rich source region in the Northern Gulf of Mexico. The genomic capacity for catabolism of multiple hydrocarbon classes in the OOV-MAG is consistent with an ability to capitalize on diffuse hydrocarbon sources that expand beyond natural seeps, including atmospheric deposition, terrestrial runoff, biogenic inputs, and oil spills. This enhanced capacity in OOV is consistent with an expanded biogeographic range relative to SV, which appears to be more highly reliant on substrate sourced from natural seepage (Supplementary Dataset S5 and Supplementary Information Fig. S9).

### **Anaerobic metabolism in *Cycloclasticus***

Anaerobic metabolism has yet to be observed in *Cycloclasticus*, and it remains unknown how these bacteria could contribute to hydrocarbon cycling in oxygen minimum zones or anoxic sediments. Here, we show the OOV-MAG of *Cycloclasticus* exhibits adaptations for life without oxygen, including the occurrence of genes for respiratory nitrate reductase (*Nar*), as well as a potential linkage to thiosulfate metabolism (Fig. 4). In OOV-MAG, we identify a complete canonical *nar* operon (*narGHJI*) encoding: i) the  $\alpha$  subunit responsible for catalyzing  $\text{NO}_3^-$  reduction to  $\text{NO}_2^-$  (*narG*); ii) the iron and sulfur-containing  $\beta$  subunit (*narH*) that transfers electrons to the molybdenum cofactor of *narG*; iii) the *narJ* chaperone used in enzyme formation and iv) the transmembrane  $\gamma$  subunit (*narI*) involved in electron transfer from membrane quinols to *narH*. Phylogenetic placement of *Cycloclasticus narG* sequences also confirms the relation to *narG* reference sequences (Supplementary Information Fig. S1).

OOV-MAG also contains the *sox* operon (*soxCDXYZAB*), which encodes periplasmic sulfur-oxidizing proteins (Fig. 4). This operon can be used as a means of detoxification in some *Gammaproteobacteria* [8]; however, we do not exclude the possibility that *Cycloclasticus* could employ a lithoheterotrophic strategy. The use of thiosulfate to supplement heterotrophy is a strategy that has been demonstrated in other *Proteobacteria* and could be useful in seeps and other benthic environments [77]. It is unclear how members of *Cycloclasticus* may access *n*-pentane in the absence of oxygen. No enzymes related to alkyl succinate synthase were detected. Multiple putative hits for the DMSO protein superfamily were detected, and this superfamily encompasses a variety of functions, including the anaerobic alkane degradation enzyme, alkane C2 methylene hydroxylase; however, OOV-MAG sequences do not form a monophyletic clade with reference sequences of this function (data not shown).

### **Deepwater Horizon *Cycloclasticus***

The microbial response to the 2010 Deepwater Horizon blowout in the Gulf of Mexico induced blooms of *Cycloclasticus* in the deep ocean from large-scale intrusions of dissolved hydrocarbons [78]. These DWH blooms included multiple *Cycloclasticus* 16S rRNA gene sequence variants, which led us to ask whether SV and OOV were among those DWH variants [71]. We analyzed the 16S rRNA gene content and conducted high-throughput sequencing on a sample collected while active flow occurred from the wellhead into the GOM. At the depth the sample was collected, there was an oxygen anomaly characteristic of the respiratory response associated with the DWH subsurface intrusions [79] (Supplementary Information Fig. S6). Upon initial analysis of the microbial community via the V4 region (252 bp) of the 16S rRNA gene, we found the SV-MAG to be identical to the dominant member of the DWH sample and OOV-MAG to be identical to the second most abundant *Cycloclasticus* 16S rRNA single nucleotide variant (Fig. 2a).

Using read-recruitment of metagenomic sequences from the same sample, we find that the fraction of the SV-MAG covered by the DWH reads spans 98% of the MAG with approximately 180X coverage. The OOV-MAG is 100% covered from reads mapped from the DWH sample with approximately 21X coverage (Supplementary Dataset S5). We reconstructed a high-quality metagenome, here named “MAG\_DWH\_1”, which is 94% complete and 3.3% redundant. Upon expanding our analysis to the full-length 16S rRNA gene (as opposed to the V4 region in Fig 2), we find that the SV-MAG is 99.5% identical to MAG\_DWH\_1. Through a phylogenomic analysis of 16 ribosomal proteins, we find MAG\_DWH\_1 forms a monophyletic clade with SV-MAG (Fig. 5a, Supplementary Information Fig. S4). For comparison, we also drew from our previously published single amplified genomes (SAGs) from DWH, which are 71%, 49%, and 46% complete and herein referred to as “SAG\_DWH\_3”, “SAG\_DWH\_1”, and “SAG\_DWH\_2” [15]. We find that “SAG\_DWH\_1” and “SAG\_DWH\_3” are closely related to OOV-MAG, whereas “SAG\_DWH\_2” appears to be related to SV-MAG (Supplementary Information Fig. S4). For the relation of SV and OOV to the SAGs and MAG\_DWH\_1, we also find supporting evidence in the analysis of Average Nucleotide Identity and the 16S gene rRNA phylogeny (Supplementary Information Fig. S4 and S5). These results indicate a previously unrecognized distinction in the microbial response to the DWH event – that SV-like *Cycloclasticus* may have responded specifically to the highly abundant soluble *n*-alkanes. In contrast, OOV-like *Cycloclasticus* may have responded to soluble *n*-alkanes and other components, including benzene and toluene.

To further assess the ecological relevance of SV and OOV *Cycloclasticus* to DWH, we compared the similarities in the *phm* phylogenetic placement between SV- and OOV-MAGs and previously published transcripts from DWH subsurface plumes (Fig. 4) [80]. These results indicate that *phm* genes most closely related to SV and OOV *Cycloclasticus* were expressed at high relative abundance during the DWH event, consistent with data

showing the rapid microbial response by *Cycloclasticus* to short-chain n-alkanes (but not methane) concurrent with active discharge [78]. The pulse of bacterial growth in the deep ocean from the DWH event has been estimated at  $> 10^{23}$  cells, with a substantial fraction being SV *Cycloclasticus*. We, therefore, questioned if this level of ecological disturbance might have structured the hydrocarbon-degrading community in the GOM through 2015 when samples for this work were collected. More data is needed to assess this hypothesis rigorously. Other researchers did find that methanotrophic biomass remained elevated in the years following the DWH event, perpetuating elevated methanotrophic activity above the background levels existing before the disaster [81]. Therefore, it remains possible that the *Cycloclasticus* observed in our pentane incubations was poised to bloom five years following the spill due to some form of memory effect from the large influx of biomass caused by the disaster.

### **Hydrocarbon metabolism across *Cycloclasticus***

To understand how hydrocarbon metabolic capability within *Cycloclasticus* relates to ecological and evolutionary patterns, we reconstructed *Cycloclasticus* MAGs from various environments using publicly available datasets (Supplementary Dataset S4). This effort resulted in eight high-quality MAGs with completion of  $>80\%$  and  $<2\%$  redundancy. These eight MAGs are in addition to the five pentane MAGs and the one DWH-MAG already discussed and includes one from the uncontaminated North Sea “NS\_1”, six from a coastal salt marsh in Skidaway Island, Georgia, “CSM\_1”, “CSM\_2”, “CSM\_3”, “CSM\_4”, “CSM\_5”, and “CSM\_6”, and one MAG from coastal seawater near Pivers Island, North Carolina “CSW\_1”. The 14 MAGs reconstructed for this study, along with other publicly available genomes, were used to form a phylogenomic tree of all *Cycloclasticus* (Fig. 5a). Each genome was then scanned for hydrocarbon-related pathways of interest and other metabolic functions related to energy generation (Fig. 5b).

From the phylogenetic analysis of ribosomal proteins alongside metabolic data, we observe distinct strategies by each major clade within the *Cycloclasticus* genera (Fig. 5b). All cultivated *Cycloclasticus* are very closely related to each other (Fig. 5a, bottom clade, denoted “isolates”). We found no evidence of genes for consuming short-chain alkanes within this clade. This is a major bias in our understanding of *Cycloclasticus*, because all other *Cycloclasticus* MAGs analyzed contained *phmo* genes. We also observe two water-column clades from uncontaminated seawater that harbor diverse pathways for short-chain and long-chain alkanes, as well as near-complete pathways for naphthalene and xylene, and complete pathways for toluene and benzene consumption. Altogether, we find a minimum of seven clades within the *Cycloclasticus*, seemingly unified as marine organisms that grow from aqueous soluble hydrocarbons. One key factor distinguishing the clades is the evolved preference to access certain classes of aqueous soluble hydrocarbons and not others.

## Conclusion

Our study provides genomic and proteomic evidence for *n*-pentane metabolism by free-living members of the *Cycloclasticus* genus in contrasting oceanic regimes, one with prolific natural seep influence and another farther removed from prolific seepage. By comparing *Cycloclasticus* genomes and MAGs, we show that the hydrocarbon metabolism within this genus is not limited to PAH degradation, with genomic variability enabling different ecotypes to access different ecological niches and structural classes of hydrocarbons. The apparent commonality among *Cycloclasticus* is not the ability to consume aromatic hydrocarbons, as the genus name suggests, but rather a metabolic specialization among the subset of hydrocarbons that exhibit aqueous solubility in marine settings.

Our results further expand on previous findings, illuminating the contrasting strategies between cultivated members of *Cycloclasticus* relying solely on aromatic hydrocarbons and mussel and sponge symbionts primarily consuming short-chain alkanes. We identify distinct clades of free-living *Cycloclasticus* that further expand on these contrasting specializations: a seep variant clade that selectively targets short-chain alkanes using *phmo*, and an open ocean variant clade that exhibits broader hydrocarbon versatility and the ability for anaerobic metabolism. A versatile metabolism could benefit *Cycloclasticus* in the ephemeral natural seep environment or in accessing non-seep hydrocarbon sources.

The specialization of SV *Cycloclasticus* on short-chain alkanes is more perplexing because of the apparent ecological risk. The apparent strategy of these SV *Cycloclasticus* requires a consistent supply of short-chain alkanes for growth, which are supplied almost exclusively from petroleum-rich environments such as seeps or spills. Given the geographic constraints on petroleum seepage and the ephemeral nature of discharge, it is perhaps surprising that specialist bacterioplankton have evolved into this niche. Nonetheless, the results of our experiments and the evident success of SV *Cycloclasticus* during DWH indicate that such specialization results in a successful ecological strategy. The success of SV *Cycloclasticus* is likely related to rapid cellular respiration that enables competitive growth upon exposure to the substrate.

The insight gained from this work provides a new vantage for considering the deep ocean microbial response to hydrocarbon discharge during DWH. SV *Cycloclasticus* was well adapted to bloom in response to the massive intrusions of aqueous-soluble *n*-alkanes that accompanied this event. The OOV *Cycloclasticus* may have engaged in direct competition by consuming these same compounds, but they may have also accessed other compounds in parallel or in sequence. This work goes beyond the DWH and provides a predictive capacity for understanding the ocean's response to future industrial incidents on

a variety of scales, such as a rupture of a subsea pipeline or the sinking of a tanker vessel carrying gas condensate, light crude oil, or diluted bitumen; or another well blowout.

### Data Availability

The datasets generated during and/or analyzed during the current study are available in the NCBI repository under the accessions PRJNA698236, SRR29495059-SRR29495064, ASM4074301v1, ASM4074303v1, ASM4074306v1, ASM4074308v1, ASM4074313v1, and ASM4074315v1. The mass spectrometry data are deposited to the Proteome Xchange Consortium via the PRIDE partner repository with the dataset identifier PXD022428 (username: [reviewer\\_pxd052872@ebi.ac.uk](mailto:reviewer_pxd052872@ebi.ac.uk); password: CX6cTbIzsFig).

### Acknowledgments

We want to thank Dr. Alison Buchan, Dr. Andrew Steen, and Dr. Lauren Quigley for their effort in collecting, sequencing, and making data publicly available from the Groves Creek Marsh in Georgia. We thank the R/V Atlantis captain and crew for their support at sea. This work used the Bridges-2 system for bioinformatic analyses, supported by NSF award number OAC-1928147 at the Pittsburgh Supercomputing Center (PSC). We thank David O'Neal and TJ Olesky for their assistance with bioinformatics optimization and support on the Bridges and Bridges-2 systems. This project was supported by NSF grant numbers OCE-1634478, OCE-1756947, and OCE-2126625.

**Competing interests:** The authors declare no competing interests.

### References

1. Reddy CM, Arey JS, Seewald JS, Sylva SP, Lemkau KL, Nelson RK, et al. Composition and fate of gas and oil released to the water column during the Deepwater Horizon oil spill. *Proceedings of the National Academy of Sciences* 2012; **109**: 20229–20234.
2. Ryerson TB, Camilli R, Kessler JD, Kujawinski EB, Reddy CM, Valentine DL, et al. Chemical data quantify Deepwater Horizon hydrocarbon flow rate and environmental distribution. *Proc Natl Acad Sci U S A* 2012; **109**: 20246–20253.
3. Gros J, Socolofsky SA, Dissanayake AL, Jun I, Zhao L, Boufadel MC, et al. Petroleum dynamics in the sea and influence of subsea dispersant injection during Deepwater Horizon. *Proc Natl Acad Sci U S A* 2017; **114**: 10065–10070.

4. Sikkema J, de Bont JA, Poolman B. Mechanisms of membrane toxicity of hydrocarbons. *Microbiol Rev* 1995; **59**: 201–222.
5. Van Hamme JD, Singh A, Ward OP. Recent Advances in Petroleum Microbiology. *Microbiology and Molecular Biology Reviews* 2003; **67**: 503–549.
6. Hara A, Syutsubo K, Harayama S. Alcanivorax which prevails in oil-contaminated seawater exhibits broad substrate specificity for alkane degradation. *Environ Microbiol* 2003; **5**: 746–753.
7. Yakimov MM, Timmis KN, Golyshin PN. Obligate oil-degrading marine bacteria. *Curr Opin Biotechnol* 2007; **18**: 257–66.
8. Valentine DL, Mezić I, Maćešić S, Črnjarić-Žic N, Ivić S, Hogan PJ, et al. Dynamic autoinoculation and the microbial ecology of a deep water hydrocarbon irruption. *Proc Natl Acad Sci U S A* 2012; **109**: 20286–91.
9. Mahmoudi N, Robeson MS, Castro HF, Fortney JL, Techtmann SM, Joyner DC, et al. Microbial community composition and diversity in Caspian Sea sediments. *FEMS Microbiol Ecol* 2015; **91**: 1–11.
10. Techtmann SM, Fortney JL, Ayers KA, Joyner DC, Linley TD, Pfiffner SM, et al. The unique chemistry of Eastern Mediterranean water masses selects for distinct microbial communities by depth. *PLoS One* 2015; **10**: 1–22.
11. Liu J, Techtmann SM, Woo HL, Ning D, Fortney JL, Hazen TC. Rapid Response of Eastern Mediterranean Deep Sea Microbial Communities to Oil. *Sci Rep* 2017; **7**: 5762.
12. McGenity TJ, McKew BA, Lea-Smith DJ. Cryptic microbial hydrocarbon cycling. *Nat Microbiol* 2021; **6**: 419–420.
13. Lea-Smith DJ, Biller SJ, Davey MP, Cotton CAR, Sepulveda BMP, Turchyn A V., et al. Contribution of cyanobacterial alkane production to the ocean hydrocarbon cycle. *Proc Natl Acad Sci U S A* 2015; **112**: 13591–13596.
14. Moulin SLY, Beyly-Adriano A, Cuié S, Blangy S, Légeret B, Floriani M, et al. Fatty acid photodecarboxylase is an ancient photoenzyme that forms hydrocarbons in the thylakoids of algae. *Plant Physiol* 2021; **186**: 1455–1472.
15. Rubin-Blum M, Antony CP, Borowski C, Sayavedra L, Pape T, Sahling H, et al. Short-chain alkanes fuel mussel and sponge *Cycloclasticus* symbionts from deep-sea gas and oil seeps. *Nat Microbiol* 2017; **2**: 17093.
16. Saunio M, R. Stavert A, Poulter B, Bousquet P, G. Canadell J, B. Jackson R, et al. The global methane budget 2000-2017. *Earth Syst Sci Data* 2020; **12**: 1561–1623.
17. Coulon F, McKew BA, Osborn AM, McGenity TJ, Timmis KN. Effects of temperature and biostimulation on oil-degrading microbial communities in temperate estuarine waters. *Environ Microbiol* 2007; **9**: 177–186.
18. Love CR, Arrington EC, Gosselin KM, Reddy CM, Van Mooy BAS, Nelson RK, et al. Microbial production and consumption of hydrocarbons in the global ocean. *Nat Microbiol* 2021; **6**: 489–498.
19. Jordan SFA, Gräwe U, Treude T, Lee EM, Schneider von Deimling J, Rehder G, et al. Pelagic methane sink enhanced by benthic methanotrophs ejected from a gas seep. *Geophys Res Lett* 2021; **63**: 183–229.
20. Jordan SFA, Gräwe U, Treude T, Lee EM van der, Deimling JS von, Rehder G, et al. Pelagic Methane Sink Enhanced by Benthic Methanotrophs Ejected From a Gas Seep. *Geophys Res Lett* 2021; **48**: e2021GL094819.

21. Button DK, Robertson BR, Lepp PW, Schmidt TM. A small, dilute-cytoplasm, high-affinity, novel bacterium isolated by extinction culture and having kinetic constants compatible with growth at ambient concentrations of dissolved nutrients in seawater. *Appl Environ Microbiol* 1998; **64**: 4467–4476.
22. Chung WK, King GM. Isolation, Characterization, and Polyaromatic Hydrocarbon Degradation Potential of Aerobic Bacteria from Marine Macrofaunal Burrow Sediments and Description of *Lutibacterium anuloderans* gen. nov., sp. nov., and *Cycloclasticus spirillensus* sp. nov. *Appl Environ Microbiol* 2001; **67**: 5585–5592.
23. Fernández-Martínez J, Pujalte MJ, García-Martínez J, Mata M, Garay E, Rodríguez-Valera F. Description of *Alcanivorax venustensis* sp. nov. and reclassification of *Fundibacter jadensis* DSM 12178T (Bruns and Berthe-Corti 1999) as *Alcanivorax jadensis* comb. nov., members of the emended genus *Alcanivorax*. *Int J Syst Evol Microbiol* 2003; **53**: 331–338.
24. MacDonald IR, Garcia-Pineda O, Beet A, Daneshgar Asl S, Feng L, Graettinger G, et al. Natural and unnatural oil slicks in the Gulf of Mexico. *J Geophys Res Oceans* 2015; **120**: 8364–8380.
25. Geiselbrecht AD, Hedlund BP, Tichi MA, Staley JT. Isolation of marine polycyclic aromatic hydrocarbon (PAH)-degrading *Cycloclasticus* strains from the Gulf of Mexico and comparison of their PAH degradation ability with that of Puget Sound *Cycloclasticus* strains. *Appl Environ Microbiol* 1998; **64**: 4703–4710.
26. Teira E, Lekunberri I, Gasol JM, Nieto-Cid M, Álvarez-Salgado XA, Figueiras FG. Dynamics of the hydrocarbon-degrading *Cycloclasticus* bacteria during mesocosm-simulated oil spills. *Environ Microbiol* 2007; **9**: 2551–2562.
27. Kasai Y, Kishira H, Harayama S. Bacteria belonging to the genus *Cycloclasticus* play a primary role in the degradation of aromatic hydrocarbons released in a marine environment. *Appl Environ Microbiol* 2002; **68**: 5625–5633.
28. Wang W, Wang L, Shao Z. Polycyclic aromatic hydrocarbon (PAH) degradation pathways of the obligate marine PAH degrader *Cycloclasticus* sp. strain P1. *Appl Environ Microbiol* 2018; **84**.
29. Zhou Z, Liu Y, Pan J, Cron BR, Toner BM, Anantharaman K, et al. Gammaproteobacteria mediating utilization of methyl-, sulfur- and petroleum organic compounds in deep ocean hydrothermal plumes. *ISME Journal* 2020; **14**: 3136–3148.
30. Cui Z, Xu G, Gao W, Li Q, Yang B, Yang G, et al. Isolation and characterization of *Cycloclasticus* strains from Yellow Sea sediments and biodegradation of pyrene and fluoranthene by their syntrophic association with *Marinobacter* strains. *Int Biodeterior Biodegradation* 2014; **91**: 45–51.
31. Button DK, Schut F, Quang P, Martin R, Robertson BR. Viability and Isolation of Marine Bacteria by Dilution Culture: Theory, Procedures, and Initial Results. *Appl Environ Microbiol* 1993; **59**: 881–891.
32. Dyksterhouse SE, Gray JP, Herwig RP, Lara JC, Staley JT. *Cycloclasticus pugetii* gen. nov., sp. nov., an Aromatic hydrocarbon- degrading bacterium from marine sediments. *Int J Syst Bacteriol* 1995; **45**: 116–123.
33. Tripp HJ. Counting marine microbes with Guava Easy-Cyte 96 well plate reading flow cytometer. *Protoc Exch* 2008.
34. Kozich JJ, Westcott SL, Baxter NT, Highlander SK, Schloss PD. Development of a dual-index sequencing strategy and curation pipeline for analyzing amplicon

- sequence data on the miseq illumina sequencing platform. *Appl Environ Microbiol* 2013; **79**: 5112–5120.
35. Apprill A, McNally S, Parsons R, Weber L. Minor revision to V4 region SSU rRNA 806R gene primer greatly increases detection of SAR11 bacterioplankton. *Aquatic Microbial Ecology* 2015; **75**: 129–137.
  36. Parada AE, Needham DM, Fuhrman JA. Every base matters: Assessing small subunit rRNA primers for marine microbiomes with mock communities, time series and global field samples. *Environ Microbiol* 2016; **18**: 1403–1414.
  37. Wear EK, Wilbanks EG, Nelson CE, Carlson CA. Primer selection impacts specific population abundances but not community dynamics in a monthly time-series 16S rRNA gene amplicon analysis of coastal marine bacterioplankton. *Environ Microbiol* 2018; **20**: 2709–2726.
  38. Callahan BJ, McMurdie PJ, Rosen MJ, Han AW, Johnson AJA, Holmes SP. DADA2: High-resolution sample inference from Illumina amplicon data. *Nature Methods* 2016 *13*:7 2016; **13**: 581–583.
  39. Pruesse E, Quast C, Knittel K, Fuchs BM, Ludwig W, Peplies J, et al. SILVA: a comprehensive online resource for quality checked and aligned ribosomal RNA sequence data compatible with ARB. *Nucleic Acids Res* 2007; **35**: 7188–7196.
  40. Glöckner FO, Yilmaz P, Quast C, Gerken J, Beccati A, Ciuprina A, et al. 25 years of serving the community with ribosomal RNA gene reference databases and tools. *J Biotechnol* . 2017. Elsevier. , **261**: 169–176
  41. Bolger AM, Lohse M, Usadel B. Trimmomatic: a flexible trimmer for Illumina sequence data. *Bioinformatics* 2014; **30**: 2114–2120.
  42. Joshi N, Fass J. Sickel: A sliding-window, adaptive, quality-based trimming tool for FastQ files (Version 1.33) [Software]. Available at <https://github.com/najoshi/sickle> 2011; 2011.
  43. Hug LA, Thomas BC, Sharon I, Brown CT, Sharma R, Hettich RL, et al. Critical biogeochemical functions in the subsurface are associated with bacteria from new phyla and little studied lineages. *Environ Microbiol* 2016; **18**: 159–173.
  44. Olm MR, Brown CT, Brooks B, Banfield JF. dRep: a tool for fast and accurate genomic comparisons that enables improved genome recovery from metagenomes through de-replication. *ISME J* 2017; **11**: 2864–2868.
  45. Nurk S, Meleshko D, Korobeynikov A, Pevzner PA. metaSPAdes: a new versatile metagenomic assembler. *Genome Res* 2017; **27**: 824–834.
  46. Gurevich A, Saveliev V, Vyahhi N, Tesler G. QUAST: quality assessment tool for genome assemblies. *Bioinformatics* 2013; **29**: 1072–1075.
  47. Langmead B, Salzberg SL. Fast gapped-read alignment with Bowtie 2. *Nature Methods* 2012 *9*:4 2012; **9**: 357–359.
  48. Langmead B, Salzberg SL. Fast gapped-read alignment with Bowtie 2. *Nature Methods* 2012 *9*:4 2012; **9**: 357–359.
  49. Li H, Handsaker B, Wysoker A, Fennell T, Ruan J, Homer N, et al. The Sequence Alignment/Map format and SAMtools. *Bioinformatics* 2009; **25**: 2078–2079.
  50. Eren AM, Esen ÖC, Quince C, Vineis JH, Morrison HG, Sogin ML, et al. Anvi'o: an advanced analysis and visualization platform for 'omics data. *PeerJ* 2015; **3**: e1319.
  51. Kim D, Song L, Breitwieser FP, Salzberg SL. Centrifuge: rapid and sensitive classification of metagenomic sequences. *Genome Res* 2016; **26**: 1721–1729.

52. Parks DH, Imelfort M, Skennerton CT, Hugenholtz P, Tyson GW. CheckM: assessing the quality of microbial genomes recovered from isolates, single cells, and metagenomes. *Genome Res* 2015; **25**: 1043–1055.
53. Chaumeil P-A, Mussig AJ, Hugenholtz P, Parks DH. GTDB-Tk: a toolkit to classify genomes with the Genome Taxonomy Database. *Bioinformatics* 2020; **36**: 1925–1927.
54. Rodriguez-R LM, Konstantinidis KT. The enveomics collection: a toolbox for specialized analyses of microbial genomes and metagenomes. *PeerJ Prepr* 2016; **4**: e1900v1.
55. Kang DD, Li F, Kirton E, Thomas A, Egan R, An H, et al. MetaBAT 2: An adaptive binning algorithm for robust and efficient genome reconstruction from metagenome assemblies. *PeerJ* 2019; **2019**: e7359.
56. Murat Eren A, Kiefl E, Shaiber A, Veseli I, Miller SE, Schechter MS, et al. Community-led, integrated, reproducible multi-omics with anvi'o.
57. Hyatt D, Chen GL, LoCascio PF, Land ML, Larimer FW, Hauser LJ. Prodigal: Prokaryotic gene recognition and translation initiation site identification. *BMC Bioinformatics* 2010; **11**: 1–11.
58. Eddy SR. Accelerated profile HMM searches. *PLoS Comput Biol* 2011; **7**: e1002195.
59. El-Gebali S, Mistry J, Bateman A, Eddy SR, Luciani A, Potter SC, et al. The Pfam protein families database in 2019. *Nucleic Acids Res* 2019; **47**: D427–D432.
60. Haft DH, Selengut JD, Richter RA, Harkins D, Basu MK, Beck E. TIGRFAMs and genome properties in 2013. *Nucleic Acids Res* 2013; **41**.
61. Aramaki T, Blanc-Mathieu R, Endo H, Ohkubo K, Kanehisa M, Goto S, et al. KofamKOALA: KEGG Ortholog assignment based on profile HMM and adaptive score threshold. *Bioinformatics* 2020; **36**: 2251–2252.
62. Edgar RC. MUSCLE: a multiple sequence alignment method with reduced time and space complexity. *BMC Bioinformatics* 2004 5:1 2004; **5**: 1–19.
63. Capella-Gutiérrez S, Silla-Martínez JM, Gabaldón T. trimAl: a tool for automated alignment trimming in large-scale phylogenetic analyses. *Bioinformatics* 2009; **25**: 1972–1973.
64. Stamatakis A. RAxML version 8: a tool for phylogenetic analysis and post-analysis of large phylogenies. *Bioinformatics* 2014; **30**: 1312–1313.
65. FigTree. <http://tree.bio.ed.ac.uk/software/figtree/>. Accessed 14 Oct 2021.
66. Lagesen K, Hallin P, Rødland EA, Stærfeldt HH, Rognes T, Ussery DW. RNAmmer: Consistent and rapid annotation of ribosomal RNA genes. *Nucleic Acids Res* 2007; **35**: 3100–3108.
67. Timmins-Schiffman E, May DH, Mikan M, Riffle M, Frazar C, Harvey HR, et al. Critical decisions in metaproteomics: achieving high confidence protein annotations in a sea of unknowns. *The ISME Journal* 2017 11:2 2016; **11**: 309–314.
68. Eng JK, Jahan TA, Hoopmann MR. Comet: An open-source MS/MS sequence database search tool. *Proteomics* 2013; **13**: 22–24.
69. Nesvizhskii AI, Keller A, Kolker E, Aebersold R. A statistical model for identifying proteins by tandem mass spectrometry. *Anal Chem* 2003; **75**: 4646–4658.
70. Ma K, Vitek O, Nesvizhskii AI. A statistical model-building perspective to identification of MS/MS spectra with PeptideProphet. *BMC Bioinformatics* 2012; **13 Suppl 1**: 1–17.

71. Irber L, Pierce-Ward NT, Brown CT. Sourmash Branchwater Enables Lightweight Petabyte-Scale Sequence Search. *bioRxiv* 2022; 2022.11.02.514947.
72. Olm MR, Crits-Christoph A, Bouma-Gregson K, Firek BA, Morowitz MJ, Banfield JF. InStrain profiles population microdiversity from metagenomic data and sensitively detects shared microbial strains. *Nature Biotechnology* 2021 39:6 2021; **39**: 727–736.
73. Jordan SFA, Treude T, Leifer I, Janßen R, Werner J, Schulz-Vogt H, et al. Bubble-mediated transport of benthic microorganisms into the water column: Identification of methanotrophs and implication of seepage intensity on transport efficiency. *Sci Rep* 2020; **10**: 1–15.
74. Hamamura N, Arp DJ. Isolation and characterization of alkane-utilizing *Nocardioides* sp. strain CF8. *FEMS Microbiol Lett* 2000; **186**: 21–26.
75. Vogel AL, Thompson KJ, Straub D, Musat F, Gutierrez T, Kleindienst S. Genetic redundancy in the naphthalene-degradation pathway of *Cycloclasticus pugetii* strain PS-1 enables response to varying substrate concentrations. *FEMS Microbiol Ecol* 2024; **100**: 60.
76. White H, Huber C, Feicht R, Simon H. On a reversible molybdenum-containing aldehyde oxidoreductase from *Clostridium formicoaceticum*. *Arch Microbiol* 1993; **159**: 244–249.
77. Moran MA, Buchan A, González JM, Heidelberg JF, Whitman WB, Kiene RP, et al. Genome sequence of *Silicibacter pomeroyi* reveals adaptations to the marine environment. *Nature* 2005 432:7019 2004; **432**: 910–913.
78. Valentine DL, Kessler JD, Redmond MC, Mendes SD, Heintz MB, Farwell C, et al. Propane respiration jump-starts microbial response to a deep oil spill. *Science* 2010; **330**: 208–11.
79. Kessler JD, Valentine DL, Redmond MC, Du M, Chan EW, Mendes SD, et al. A Persistent Oxygen Anomaly Reveals the Fate of Spilled Methane in the Deep Gulf of Mexico. *Science (1979)* 2011; **331**: 312–315.
80. Rivers AR, Sharma S, Tringe SG, Martin J, Joye SB, Moran MA. Transcriptional response of bathypelagic marine bacterioplankton to the Deepwater Horizon oil spill. *The ISME Journal* 2013 7:12 2013; **7**: 2315–2329.
81. Rogener MK, Bracco A, Hunter KS, Saxton MA, Joye SB. Long-term impact of the Deepwater Horizon oil well blowout on methane oxidation dynamics in the northern Gulf of Mexico. *Elem Sci Anth* 2018; **6**: 73.

## Figure Legends



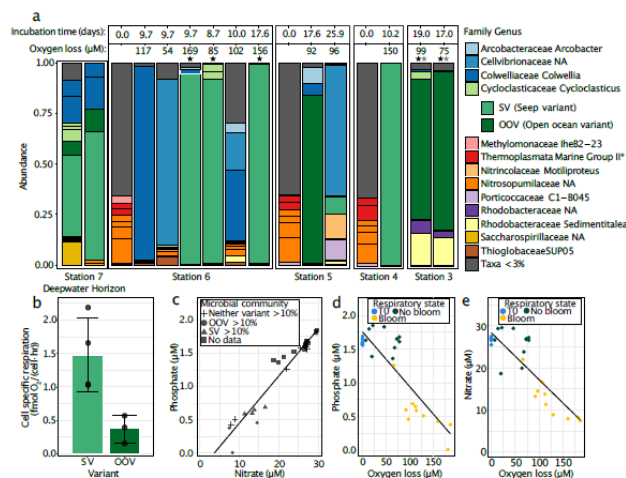


**Figure 2.** Microbial and geochemical characteristics of *n*-pentane blooms alongside environmental samples from the Deepwater Horizon event. **a** Microbial community composition informed via the V4 region of the 16S rRNA gene. Initial “T0” samples collected at the start of incubations are denoted with an incubation time of 0.0 days. *n*-pentane incubations were harvested after meeting the operational definition of bloom state (three consecutive time points were observed with oxygen loss greater than 0.21  $\mu\text{M}$ ). Deepwater Horizon environmental samples were collected on 5/30/10 during the DWH event. SV strain *Cycloclasticus* blooms in ~9-18 days in locations close to natural seepage and was abundant during the Deepwater Horizon disaster. OOV strain of *Cycloclasticus* blooms in 17-19 days and dominates seawater originating further from natural seepage inputs. \*No taxonomic representative at the family or genera level. “Oxygen loss” indicates the change in oxygen relative to initial concentrations when the DNA sample was collected after normalization to unamended controls **b** Cell-specific respiration in incubations dominated (>80%) by SV and OOV *Cycloclasticus*. **c** Dissolved phosphate vs dissolved nitrate concentration in initial samples (T0) and at sample harvest. **d** Dissolved phosphate concentration in final samples is depleted compared to unamended controls and initial samples (T0). **e** Dissolved nitrate concentration in final samples is depleted compared to unamended controls and initial samples (T0). Black and gray stars indicate metagenomic and metaproteomic samples, respectively.

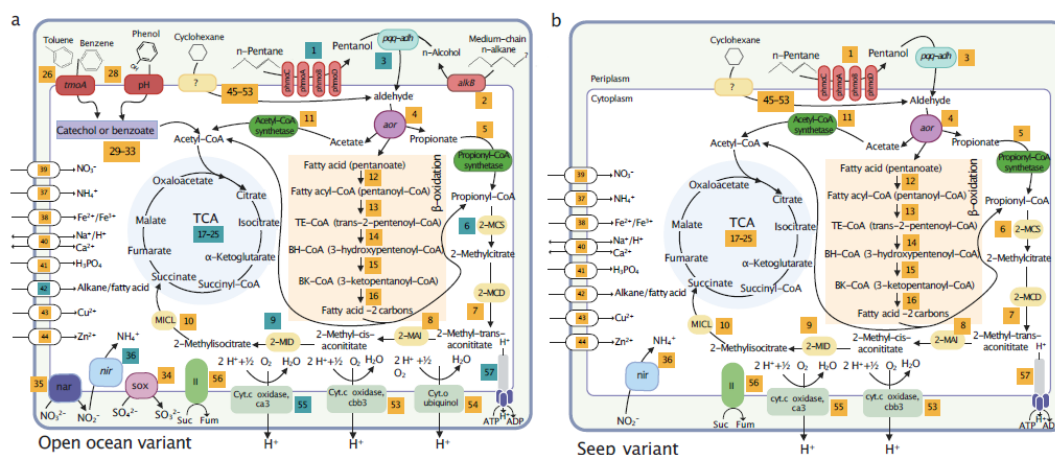


**Figure 3.** Carbon, nitrogen, and sulfur metabolism present in *Cycloclasticus* variants blooming on pentane. **a** Open ocean variant, OOV-MAG, and **b** Seep variant SV-MAG. Yellow boxes indicate a reaction (and its reference number) that could be linked with a predicted metabolic function, see Supplementary Dataset S3. Blue boxes indicate peptides for that enzyme were observed in proteomic data. Proteomics performed on only OOV-MAG. If the reaction box describes multiple enzymes, only one needs to be observed in proteomic data for it to be colored blue. Enzyme abbreviations: particulate hydrocarbon monooxygenase *phmo* (A, B, C, D); PQQ-dependent alcohol dehydrogenase (*pqq-adh*); aldehyde oxidoreductase (*aor*); 2-methylcitrate synthase (*2-mcs*); 2-methylcitrate dehydratase (*2-MCD*); 2-methylcitrate isomerase (*2-MAI*); 2-methylisocitrate dehydratase (*2-MID*); methylisocitrate lyase (*MICL*); nitrite reductase (*Nir*); respiratory nitrate reductase (*Nar*); thiosulfate oxidation complex (*Sox*); alkane-1-monooxygenase (*alkB*); toluene monooxygenase (*tmoA*); phenol/toluene 2-monooxygenase (*pH*). The tricarboxylic acid (TCA) and beta-oxidation pathway are highlighted in blue and peach colors.

UNCORRECTED

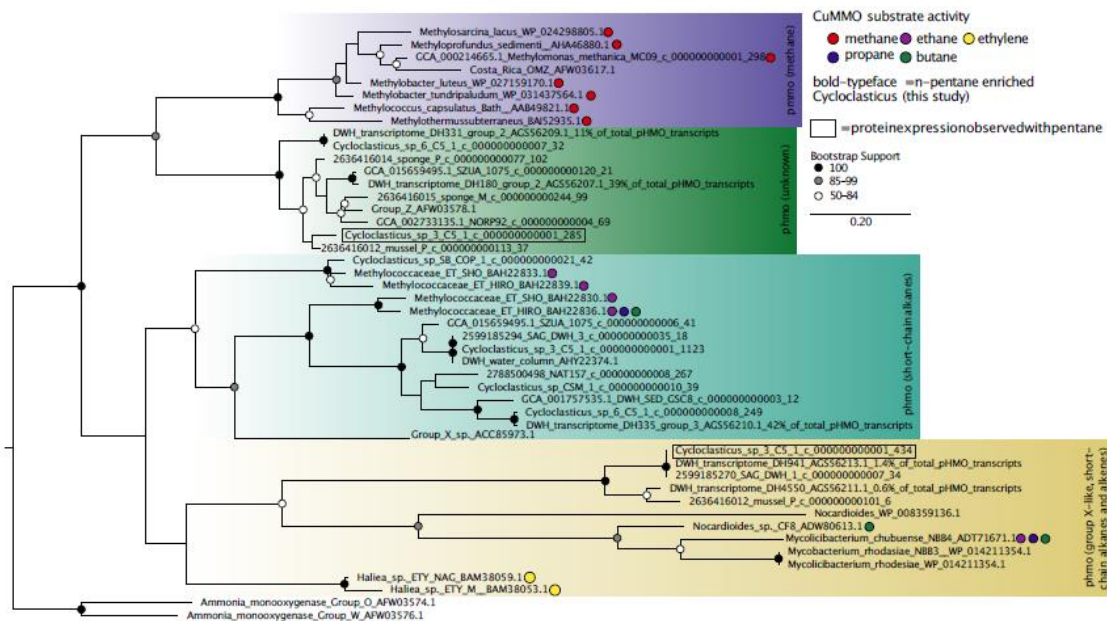


**Figure 4.** Maximum likelihood tree of *phmo* subunit A drawn to scale, with branch lengths representing the number of substitutions per site. Bootstrap values below 50% are not shown. Each major clade is color-coded for readability with purple representing *phmo* with activity on methane, the green clade is lacks any known substrate specificity and is thus labeled 'unknown', the cyan clade represents group X *phmo* gene (ethane/ethylene, propane, and butane activity), and the yellow clade are group-X like (ethane, propane, and butane activity). Sequences from the pentane-enriched *Cycloclasticus* MAGs are in bold; boxed values indicate *phmo* gene detected in proteomic data.

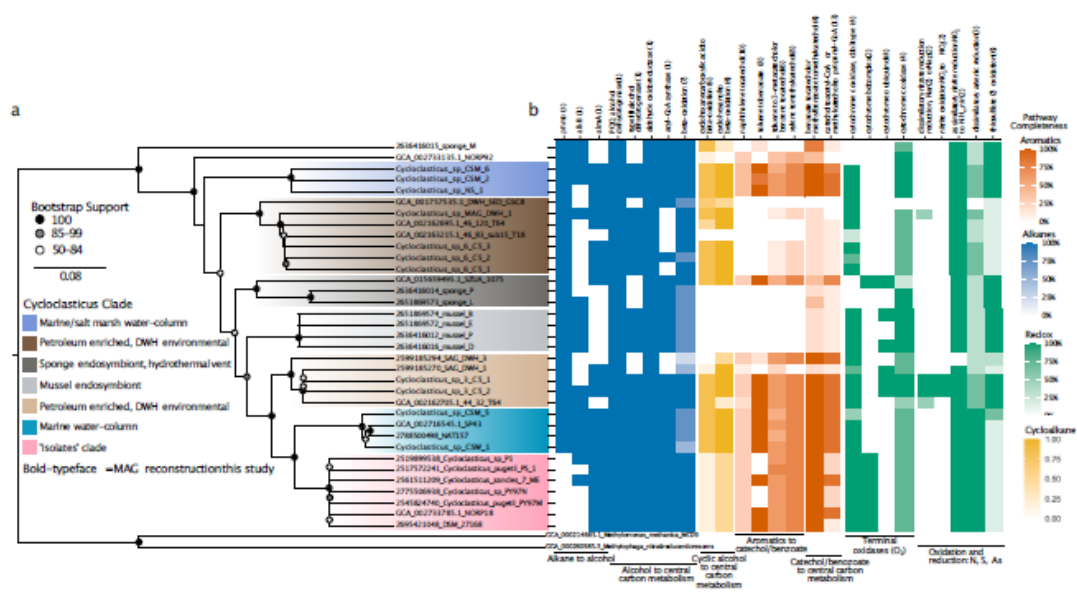


**Figure 5.** Phylogeny and capabilities for hydrocarbon consumption of *Cycloclasticus*. **a** Phylogeny constructed using 16 ribosomal proteins, subclades are designated based on relative distance from the root and supported by average nucleotide identity (Supplementary Information, Figure S5). **b** Completeness of select metabolic pathways relating to alkane (blue), aromatic (red), cycloalkane (yellow) metabolism and redox (green). The number of genes considered in calculating pathway completeness is shown in parentheses.

UNCORRECTED